Copyright © 2009 Tech Science Press CMES, vol.45, no.3, pp.207-225, 2009

A Computational Approach for Pre-Shaping Voltage Commands of Torsional Micromirrors

T. Starling[1], **M. F. Daqaq**[1] **and G. Li**[1,2]

Abstract: Input-shaping is an open-loop control technique for dynamic control of electrostatic MEMS. In MEMS applications, open-loop control is attractive as it computes a priori the required system input to achieve desired dynamic behavior without using feedback. In this work, a 3-D computational electromechanical analysis is performed to preshape the voltage commands applied to electrostatically actuate a torsional micromirror to a desired tilt angle with minimal residual oscillations. The effect of higher vibration modes on the controlled response is also investigated. It is shown that, for some structural design parameters, the first bending mode of the micromirror can have a significant effect on the dynamic response. If not accounted for in the control algorithm, these bending vibrations could have an adverse effect on the controlled response of the mirror. To resolve this issue, a numerical optimization procedure is employed to shape the input voltage from the real time dynamic response of the mirror structure. The optimization scheme yields a periodic nonlinear input voltage design that can effectively suppress the bending mode.

Keywords: MEMS, Control, Modeling, Input shaping.

1 Introduction

Within the large family of Microelectromechanical systems (MEMS) [Judy (2001)], electrostatically actuated micromirrors have been developed for many applications such as optical RF switches, microscanners and video projectors [Wen, Hoa, and Kirk (2004)]. As the potential applications of mircomirrors are very broad and promising, there is a pressing need for effective control algorithms to improve their dynamic behavior. Of special importance, is enhancing the transient response characteristics (e.g., rise time, settling time, overshoot) y using step voltage commands [Borovic, Liu, Popa, Cai, and Lewis (2005); Daqaq, Reddy, and Nayfeh

[1] Department of Mechanical Engineering, Clemson University, Clemson, SC
[2] Email: gli@clemson.edu

(2008)]. From a control perspective, there are two approaches for MEMS control: the closed- and open-loop techniques. On one hand, closed-loop control utilizes real-time feedback signals to monitor one or more of the system states, which makes it more robust and resistant to fabrication uncertainties, design imperfections, and external disturbances. However, the implementation of closed-loop algorithms for MEMS applications is very cumbersome [Borovic, Liu, Popa, Cai, and Lewis (2005)]. Unlike macro mechanical systems, the implementation of the feedback mechanism is difficult due to the small size of the system, the high speed, and high frequency operations. In addition, the closed-loop control system needs to be integrated with the MEMS system. The added control system and circuits can significantly increase the complexity and reduce the reliability of the microdevice. On the other hand, open-loop algorithms compute the required system input to achieve a desired behavior without using feedback, thereby eliminating the potential problems associated with the closed-loop control. For this reason, open-loop control of MEMS has attracted significant research interest in the past decade.

One widely used open-loop control technique is input shaping [Singer and Seering (1990)]. This technique uses a sequence of impulses to generate the desired input. When these impulses are convolved with the original input to the system, they result in zero residual vibrations. Recently input-shaping has also been used in input voltage design to control MEMS devices such as electrostatic comb drives [Borovic, Hong, Liu, Xie, and Lewis (2005)], thermal bimorph MEMS [Popa, Byoung, Wen, Stephanou, Skidmore, and Geisberger (2003)] and electrostatically actuated microbeams [Yang, Chen, Lee, and Yin (2006); Lin (2009)]. The performance of closed-loop and open-loop control approaches have been compared in [Borovic, Liu, Popa, Cai, and Lewis (2005)]. For electrostatic micromirrors, an input-shaping control algorithm based on analytical lumped models has also been proposed recently in [Daqaq, Reddy, and Nayfeh (2008)].

While input-shaping control is attractive due to its simplicity, its effectiveness depends on the accuracy of the model used to compute the input signal. All of the above mentioned input shaping controllers are based on simplified analytical and semi-analytical models. As most MEMS devices experience large deformations and are actuated using a nonlinear energy field, it is not clear to what extent these models are accurate. In addition, as the analytical input-shaping approaches aim to suppress the first vibration mode of microsturctures, it is not clear what the effects of higher vibration modes are and whether it is possible to improve input-shaping to account for these effects.

To address these issues, accurate modeling of MEMS dynamics is required. Based on the level of abstraction, MEMS modeling approaches can be categorized into three groups: analytical/semi-analytical approach [Daqaq, Reddy, and Nayfeh (2008);

Mukherjee (2000)], reduced-order approach [Rewienski and White (2003); Bettini, Brusa, Munteanu, Specogna, and Trevisan (2008)], and full numerical approach [Li and Aluru (2003); Chen, Lai, and Liu (2009)]. Compared to the first two types of approaches, the full numerical approach solves the governing partial differential equations directly. With the trade-off of computational cost, the full numerical approach is general and more accurate. In this work, to achieve the required accuracy, we adopt the full numerical approach to investigate the input-shaping control of electrostatic micromirrors. The numerical analysis of MEMS involves a mechanical analysis and an electrostatic analysis. Towards that end, we develop a full 3-D electromechanical solver for dynamic analysis of electrostatically-actuated MEMS where the mechanical analysis is performed by using the finite element method (FEM) and the electrostatic analysis is performed by using the boundary element method (BEM). On top of the electromechanical solver, we implement an input-shaping open-loop control algorithm. The effect of higher vibration modes on the input-shaping control of electrostatic micromirrors is investigated. We show that, depending on the design parameters, the bending mode of the micromirror structure can have significant effect on the dynamic behavior of the system, which is difficult to suppress by implementing traditional step-voltage open-loop algorithms. To resolve this issue, we employ a numerical optimization procedure to shape the input voltage from the real time dynamic response of the mirror structure. The optimization procedure results in a periodic input voltage design that can effectively reduce the effect of the bending mode.

The rest of the paper is organized as follows. In Section 2, we present the micromirrors which we investigate in this work. Computational models for coupled electromechanical dynamic analysis of MEMS are presented in Section 3. The effect of higher vibrational modes on the input-shaping control of the micromirros are shown in Section 4. Section 5 describes an input-shaping optimization procedure and presents the optimized input-shaping results. Conclusions are given in Section 6.

2 Micromirros

We consider a micromirror device shown in Fig. 1. The mirror consists of two identical microbeams of length l, width w, and thickness h. The beams are fixed on one side and connected to a rigid rectangular plate (the mirror) on the other side. The mirror has a length L_m, width a and thickness h. Beneath the micromirror are two electrodes, each of length L_m and width $(a_2 - a_1)/2$. The gap between the undeformed position of the mirror and the electrodes is denoted as d. The whole microstucture is etched out of a silicon substrate that has a density ρ, a Young's Modulus E, and a Poisson's ratio, ν. The mirror is activated to rotate in either

direction by supplying a voltage $V(t)$ to the corresponding electrode. The voltage generates electric charges on the surface of the mirror and the electrode, and hence produces an attractive electrostatic force between the mirror plate and the electrode. When the mirror deforms due to the electrostatic force, the electric field between the mirror plate and the electrode changes and the electric charge redistributes, causing a change in electrostatic force. The mirror plate reaches equilibrium when the electrostatic and the mechanical forces are balanced.

We investigate the dynamic response of three different designs of the micromirror device as shown in Fig. 2. In all three design, the size of the mirror plate and the electrodes are the same. In the first design (Mirror *A*), the suspension beams are relatively short and the electrodes are positioned aligning with the outer edges of the mirror plate. The second design (Mirror *B*) has the same design parameters as those of Mirror *A* except that the electrodes are placed more towards the center. In the third design, Mirror *C*, the suspension beam length is increased and the electrodes are placed at the same positions as those in Mirror *B*. The material properties and dimensions of the mirrors are listed in Table 1.

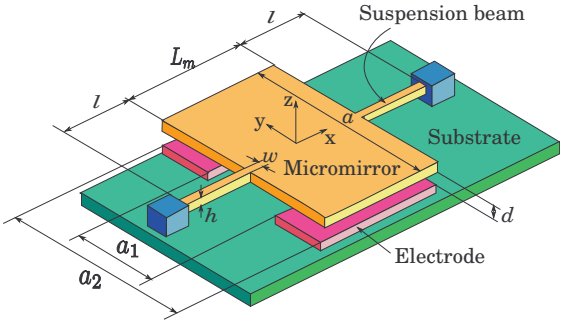

Figure 1: Schematic diagram of the torsional micromirror.

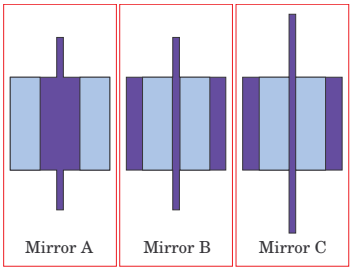

Figure 2: Dimension and electrode positions of the micromirrors.

3 Computational Modeling

The numerical analysis of electrostatic micromirrors involves coupled mechanical and electrostatic models. In the mechanical analysis, we employ the finite element method to solve the Euler-Lagrange equation of motion for the mirror structure. In the FEM, the mirror structure is discretized into elements. The displacement, velocity, and acceleration are approximated in each element by using shape functions. Since the rotation and deflection of the micromirror are in different planes

Table 1: Material properties and dimensions of the torsional micromirrors.

Properties			
Modulus of elasticity, E (GPa)	170		
Poisson's ratio	0.3		
Density, ρ (kg/m^3)	2330		
Dielectric constant of air, ε_0 (F/m)	8.85×10^{-12}		
Dimensions	Mirror A	Mirror B	Mirror C
Mirror width, a (μm)	100	100	100
Mirror length, L_m (μm)	100	100	100
Beam length, l (μm)	45	45	65
Beam width, w (μm)	1.55	1.55	2
Beam thickness, h (μm)	1.50	1.50	1.50
Electrode length, b (μm)	100	100	100
Electrode parameter, $\alpha = \frac{a_1}{a}$	0.3	0.08	0.08
Electrode parameter, $\beta = \frac{a_2}{a}$	1.0	0.78	0.78
Gap height, d (μm)	2.75	2.75	2.75

as shown in Fig. 1, a 3-D computational model is necessary. The gap between the mirror plate and the electrodes is small as shown in Table 1. Due to the pull-in effect, the actual rotation of the mirror is even smaller compared to the dimension of the mirror structure. Typically the rotation angle is less than 1^o. In this case, a linear elasticity theory can be used for the mechanical analysis [Li and Aluru (2001)]. The discretized equation of motion can be written as

$$\mathbf{M}\ddot{\mathbf{d}} + \mathbf{C}\dot{\mathbf{d}} + \mathbf{K}\mathbf{d} = \mathbf{P}. \tag{1}$$

where $\mathbf{d}$, $\dot{\mathbf{d}}$ and $\ddot{\mathbf{d}}$ are the displacement, velocity and acceleration vectors, respectively, and $\mathbf{M}$, $\mathbf{C}$, $\mathbf{K}$ are the global mass, damping, and stiffness matrices, respectively, and $\mathbf{P}$ is the force vector. The Newmark method [Cook, Malkus, Plesha, and Witt (2001)] is used to solve Eq. (1) for the elastodynamic analysis. In the Newmark method, for a time step $n+1$, the global equation of motion Eq. (1) are combined with kinematic equations of motion to compute the nodal displacement,

velocity and acceleration, i.e.,

$$\left(\mathbf{M}+\gamma\mathbf{C}\Delta t+\beta\Delta t^2\mathbf{K}\right)\ddot{\mathbf{d}}_{n+1}=$$
$$\mathbf{P}_{n+1}-(\mathbf{C}+\Delta t\mathbf{K})\dot{\mathbf{d}}_n-\left(\Delta t(1-\gamma)\mathbf{C}+\frac{\Delta t^2}{2}(1-2\beta)\mathbf{K}\right)\ddot{\mathbf{d}}_n-\mathbf{K}\mathbf{d}_n \tag{2}$$

$$\mathbf{d}_{n+1}=\mathbf{d}_n+\Delta t\dot{\mathbf{d}}_n+\frac{\Delta t^2}{2}(1-2\beta)\ddot{\mathbf{d}}_n+\frac{\Delta t^2}{2}(2\beta)\ddot{\mathbf{d}}_{n+1} \tag{3}$$

$$\dot{\mathbf{d}}_{n+1}=\dot{\mathbf{d}}_n+\Delta t(1-\gamma)\ddot{\mathbf{d}}_n+\Delta t\gamma\ddot{\mathbf{d}}_{n+1} \tag{4}$$

where γ and β are the time integration parameters. In this work, an implicit scheme with numerical smoothing ($\beta=0.3025$ and $\gamma=0.6$) is adopted [Cook, Malkus, Plesha, and Witt (2001)].

To determine the electrostatic force acting on the mirror structure, the classical potential problem defined by the Laplace equation needs to be solved in the domain exterior to the mirror structure and the electrodes. Boundary integral methods can be employed to efficiently solve Laplace-type [Li and Aluru (2002)] and Poisson-type [He, Lim, and Lim (2008)] electrostatic problems. The boundary integral equation for the Laplace-type electrostatic problem is given by [Shi, Ramesh, and Mukherjee (1995)],

$$\phi(\mathbf{p})=\int_\gamma G(\mathbf{p},\mathbf{q})\sigma(\mathbf{q})d\gamma \tag{5}$$

where σ is the unknown surface charge density, $\mathbf{p}$ is the source point, $\mathbf{q}$ is the field point, $G(\mathbf{p},\mathbf{q})$ is the Green's function and γ is the boundary of the mirror structure and the electrodes. In three-dimensions, $G(\mathbf{p},\mathbf{q})=1/(4\pi\varepsilon r(\mathbf{p},\mathbf{q}))$, where ε is the permittivity of free space, and $r(\mathbf{p},\mathbf{q})=|\mathbf{p}-\mathbf{q}|$ is the distance between the source point $\mathbf{p}$ and the field point $\mathbf{q}$. Note that Eq. (5) is defined for the deformed positions of the conductors.

In this work, the quadrilateral faces of the hexahedral finite element elements on the surface of the mirror are used as boundary elements in the electrostatic analysis. The FE and BE nodes coincide and no interpolation between them is needed. The surface charge density is assumed to be constant on each boundary element. The centroid of each element is taken as the collocation point. Equation (5) can be rewritten in a matrix form as

$$\mathbf{H}\boldsymbol{\sigma}=\boldsymbol{\phi} \tag{6}$$

where, for a total number of K boundary elements, $\mathbf{H}$ is a $K\times K$ coefficient matrix, $\boldsymbol{\phi}$ and $\boldsymbol{\sigma}$ are the $K\times 1$ prescribed potential and unknown charge density vectors,

respectively. The entries in the coefficient matrix and the vectors are given by

$$H(i,j) = \int_{\gamma_j} \frac{1}{4\pi\varepsilon r(\mathbf{p}_i, \mathbf{q}_j)} d\gamma \qquad i,j = 1,\ldots,K \tag{7}$$

$$\boldsymbol{\phi} = \left\{ \phi_1 \ \phi_2 \cdots \ \phi_K \right\}^T \qquad \boldsymbol{\sigma} = \left\{ \sigma_1 \ \sigma_2 \cdots \ \sigma_K \right\}^T \tag{8}$$

where γ_j is the area of the j-th boundary element, $\mathbf{p}_i$ is the collocation point (source point) on the i-th element and $\mathbf{q}_j$ is the field point on the j-th element. The unknown vector of surface charge density in Eq. (8) can be computed by solving the matrix problem in Eq. (6).

Numerical integration is required in computing the matrix $\mathbf{H}$ as shown in Eq. (7). When the source and field points $\mathbf{p}$ and $\mathbf{q}$ are in the same boundary element, i.e., $i = j$, the integral $H(i,j)$ becomes singular. For the $1/r$ type singular kernel, several regularization techniques are available [Aliabadi and S.Hall (1989, 1985)]. In this work, a regularising transformation integration method [Aliabadi and S.Hall (1989)] is employed for the evaluation of the singular integral. The transformation technique divides the element into triangular sub-elements then transforms the triangular element to a square plane element. The singular integral is regularized through the Jacobian generated by the transformation (see [Aliabadi and S.Hall (1989)] for more details). For $i \neq j$, regular Gaussian quadrature is used. Once the surface charge density is computed, the electrostatic surface force is obtained by $\mathbf{h} = 2(\sigma^2/\varepsilon)\mathbf{n}$ where $\mathbf{n}$ is the surface outward normal vector.

In the static coupled electromechanical analysis, the equation of motion, Eq. (1), reduces to the equation of equilibrium, $\mathbf{Kd} = \mathbf{P}$. A self-consistent analysis is performed via a relaxation iteration between the mechanical equation of equilibrium and the electrostatic equation given in Eq. (6). In the dynamic coupled electromechanical analysis, within each time step, the mechanical analysis (Eqs. (2-4)) and electrostatic analysis (Eq. (6)) are performed self-consistently. Note that, in this work, we investigate input-shaping control of micromirrors with negligible damping, i.e., $\mathbf{C}$ is set to zero.

The pull-in curves for the three micromirrors shown in Fig. 2 are computed from the static coupled analysis. Figure 3 shows the static pull-in of Mirror A. The pull-in voltage is 18.74 V. This result compares favorably with the pull-in voltage of 18.4 V obtained in [Daqaq, Reddy, and Nayfeh (2008)] where the same mirror was investigated. The static pull-in voltage of Mirror B and C are 27.4 V and 23.5 V, respectively (figures not shown). Figure 4 shows the distribution of the surface charge density on the bottom and top surfaces of the deformed mirror plate and an electrode, respectively.

Figures 5-10 show the first 6 vibrational modes of Mirror A (or Mirror B) obtained

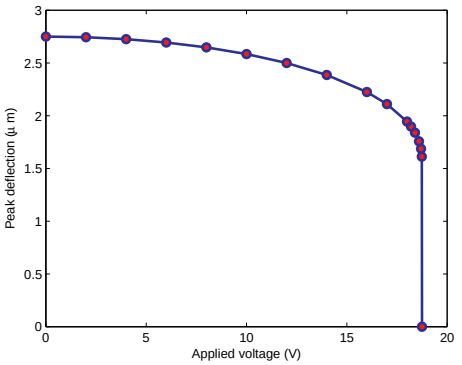

Figure 3: Static pull-in of Mirror A.

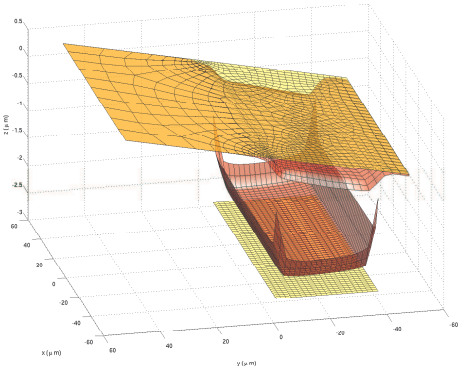

Figure 4: Surface charge density distribution on the mirror plate and the electrode(not to scale).

from the full numerical model. The frequencies of these modes at zero DC voltage are listed in Table 2. It is shown that the second vibrational mode is the bending mode with a frequency about 2.65 times the frequency of the first rotational mode. It can be observed from the figure that the third mode and above are not likely to get excited by the electrostatic force due to the structural configuration. However, since the electrostatic surface force acts normal to the mirror plate, the bending mode will be excited by the electrostatic force. Therefore, when a DC voltage is applied to the activating electrode, both of the rotational and bending modes are in action. Indeed, while uncoupled when the DC voltage is zero, the first two modes of mirror vibration are linearly and nonlinearly coupled through the electrostatic field [Daqaq, Reddy, and Nayfeh (2008)]. Therefore, one cannot excite one of these modes without exciting the other.

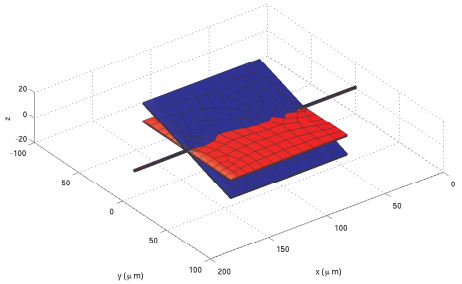

Figure 5: The 1st mode of Mirror A/B.

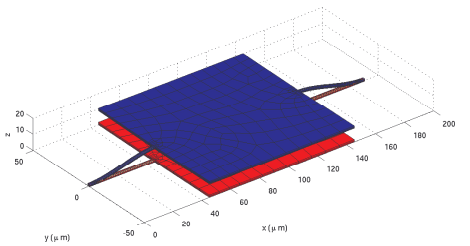

Figure 6: The 2nd mode of Mirror A/B.

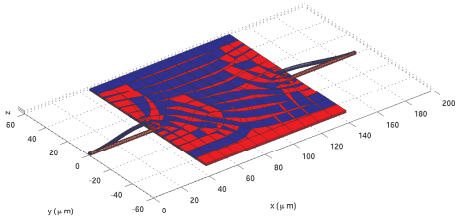

Figure 7: The 3rd mode of Mirror A/B.

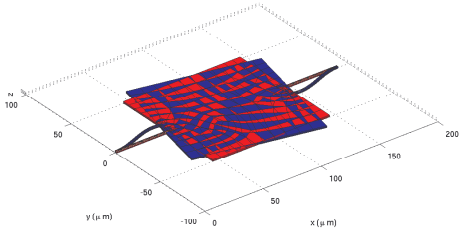

Figure 8: The 4th mode of Mirror A/B.

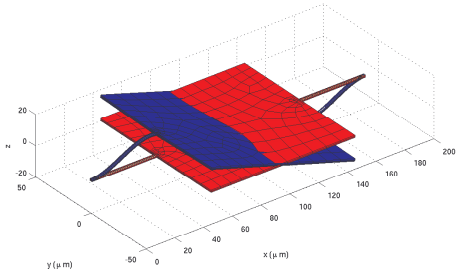

Figure 9: The 5th mode of Mirror A/B.

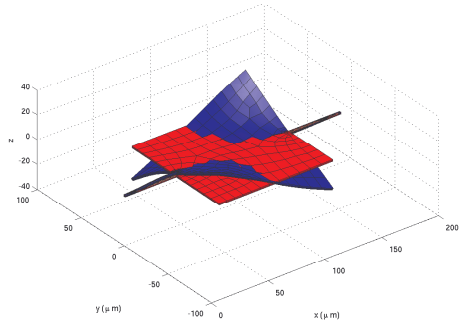

Figure 10: The 6th mode of Mirror A/B.

Table 2: Natural frequencies and periods of Mirror A/B.

Mode	1	2	3	4	5	6
Frequency (MHz)	0.047	0.126	0.137	0.246	0.317	1.473
Period (μs)	21.10	7.94	7.30	4.07	3.15	0.68

Figure 11 shows the dynamic response of Mirror C with an applied DC voltage of 20 V. When the mirror deforms, the nonlinear electrostatic force becomes larger and slows down the motion of the mirror. Hence, the time that the mirror spends close to the activating electrode is larger than that spent away from it. When the applied voltage is increased further, the mirror stays at the bottom position for a longer period of time until finally the voltage reaches a critical point at which the increase in the electrostatic force becomes faster than the increase in the mechanical restoring and inertial forces. At that point, the mirror gets pulled down to the substrate dynamically, as shown in Figure 12. The dynamic pull-in voltage of Mirror C is found to be 21.76 V which is lower than the static pull-in.

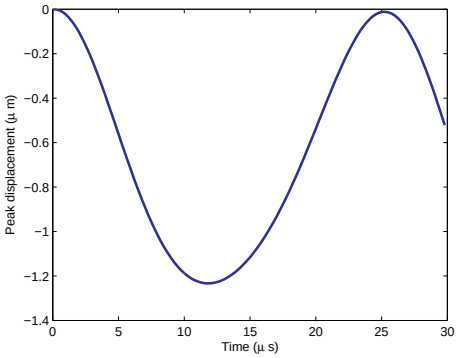

Figure 11: Dynamic response of Mirror C (20 V).

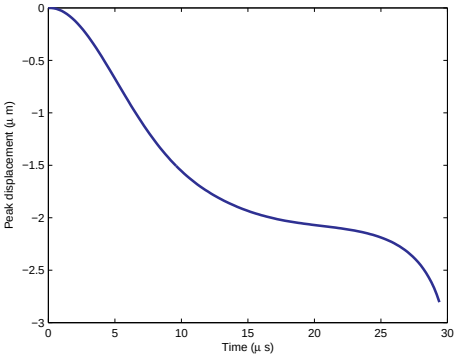

Figure 12: Dynamic pull-in of Mirror C.

4 Bending Mode Effect on Input Shaping

Torsional micromirrors are designed to accurately reflect and switch light beams from a source to a given surface. This process can be achieved by applying a DC voltage of a certain magnitude to rotate the mirror to a desired predefined tilt angle. Two important performance criteria are accurate positioning and the ability of the mirror to settle fast at the desired tilt angle. One of the major issues with applying a single step DC voltage, V_1, is the long settling time of the mirror oscillations around the desired angle especially because the damping effects are usually small. This has the adverse effect of slowing down the mirror operation significantly. To resolve this issue, one can resort to pre-shaping the voltage commands. The idea of voltage-shaping is to introduce a second step voltage V_2 right at the point where the mirror plate reaches its peak rotation angle (maximum overshoot). At that point, the angular velocity of the mirror plate is zero. If the magnitude of the second voltage step is chosen such that the static equilibrium rotation angle associated with V_2 is exactly equal to the maximum overshoot resulting from V_1, the residual vibrations go to zero after the application of V_2.

This voltage shaping algorithm assumes the presence of only one modal frequency in the response. If other modal frequencies with significant energy components are present in the response, the second voltage step V_2 will not be able to completely eliminate the residual oscillations. Convolving additional voltage impulses (more steps) to eliminate the higher vibration modes as described in the multimode input-shaping of macrosystems [Hyde (1991)] is not effective in this case due to the linear coupling between the first two modes of the mirror as described previously. This coupling appear through the input, and therefore, an additional voltage step that is

designed to eliminate the second bending mode can excite the first mode and vise versa. We address the effect of the bending mode on the response in this section and propose a technique to eliminate it in the next section.

Using the numerical model, we compute the shaped voltage input for the three micromirrors shown in Fig. 2. First, a set of dynamic simulations are performed to find the magnitude of the first voltage step V_1 which produces the desired peak tilt angle. Afterwards, a set of static analyses are performed to find the second impulse V_2 which produces the desired static tilt angle. Figure 13 shows the step voltage and the dynamic response of Mirror A. The response matches the desired behavior in the sense that the oscillation of the mirror structure after it reaches the desired angle is minimal as predicted by the semi-analytical model [Daqaq, Reddy, and Nayfeh (2008)]. However, for Mirror B, the shaped voltage input does not produce the desired dynamic behavior as shown in Fig. 14. Oscillations after the second step voltage are observed. More significantly, as shown in Fig. 14(c), the period of oscillation is measured to be about 8.3 μs which is close to the period of the bending mode of the micromirror (7.94 μs) listed in Table 2. Note that the bending mode frequency drops as the applied DC voltage increases due to the electrostatic softening effects [Daqaq, Reddy, and Nayfeh (2008)]. Therefore, it is evident that residual vibration of the micromirror is due to the bending mode. Figure 15 shows the response of Mirror C. The residual vibration is very large in this case. The period of oscillation is measured at about 13.8 μs. The period of the bending mode of undeformed Mirror C obtained from the numerical calculation is 13.0 μs. Again, this result demonstrates that the residual vibration is due to the bending mode of the micromirror structure.

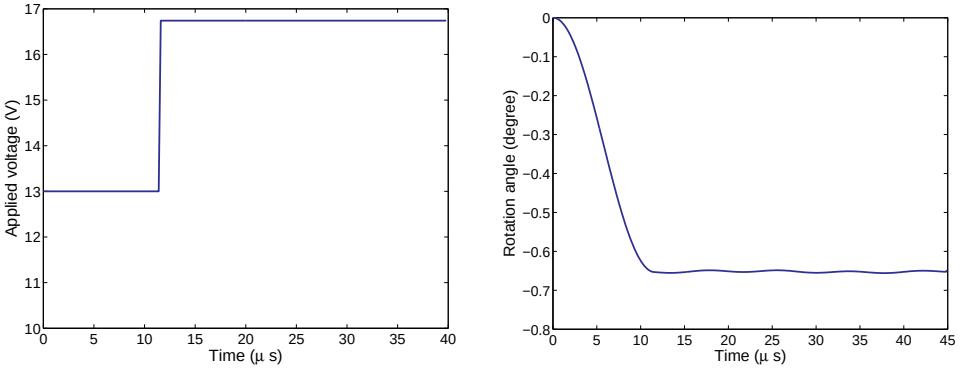

Figure 13: Step-shaped input voltage control for Mirror A. Left: step-voltage input. Right: dynamic response of the micromirror.

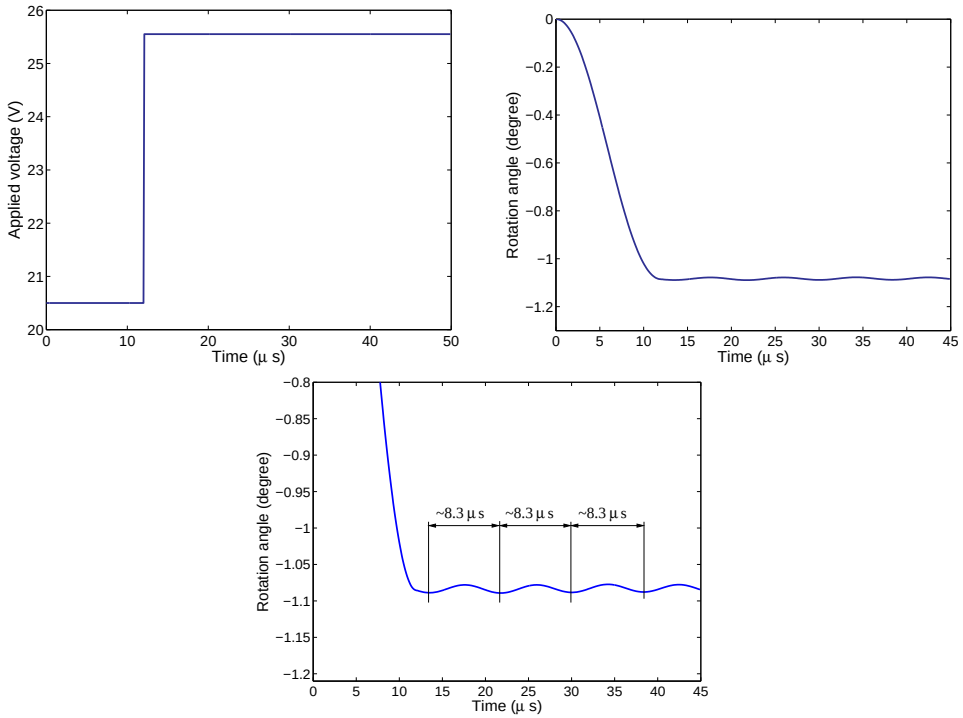

Figure 14: Step-shaped input voltage control for Mirror B. Left: step-voltage input. Right: dynamic response of the micromirror. Bottom: residual vibration of the mirror.

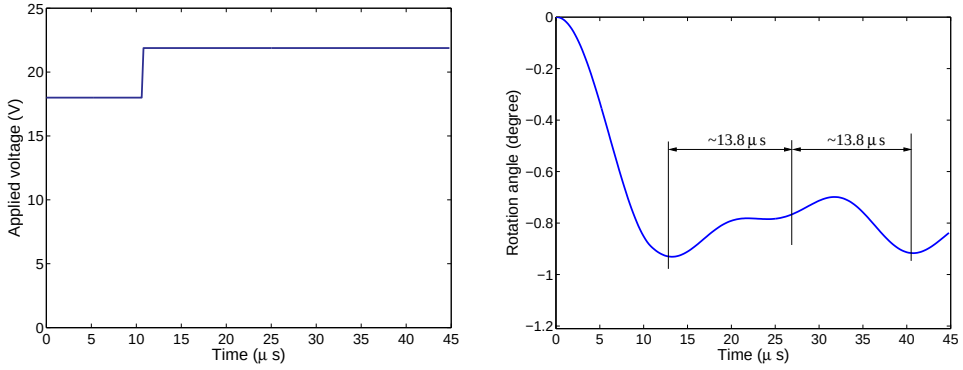

Figure 15: Step-shaped input voltage control for Mirror C. Left: step-voltage input. Right: dynamic response of the micromirror.

These results prompt further discussion on why the energy component of the bending mode is higher for Mirror B and significantly higher for Mirror C, thereby producing large residual oscillations. First, by comparing Mirror A and B, it can be noted that the electrodes in Mirror B are placed closer to the center of the mirror plate, see Table 3. Therefore, the torque/pulling force ratio is larger in Mirror A, thus the bending mode is barely excited in Mirror A and the resultant residual bending vibrations are negligible. In that case, the traditional double-step input voltage is sufficient to control the dominant torsional mode. However, for Mirror B, due to the position of the electrodes, more electrostatic energy contributes to the beam bending. Therefore, the bending mode becomes significant yielding larger bending oscillations that are not suppressed by the step actuation voltage, as shown in Fig. 14(c).

Table 3: Comparison of the torsional micromirror designs.

	Mirror A	Mirror B	Mirror C
Distance of electrodes to the center (μm)	32.5	21.5	21.5
Bending Stiffness (N/m)	19.52	19.52	8.36
Torsional Stiffness (Nm)	2.22e-9	2.22e-9	2.47e-9

Second, by comparing Mirror C and B, it is noted that the geometry of the suspension beams changes while all the other design parameters are kept constant. The change in the geometry of the suspension beams changes the ratio of their torsional/bending stiffness. Specifically, the bending stiffness of the beams can be determined by [Daqaq, Reddy, and Nayfeh (2008)]

$$K_B = \frac{24EI_y}{(2l)^3} \tag{9}$$

where E is the Young's modulus, $I_y = wh^3/12$ is the moment of inertia of the suspension beam cross section about the y-axis, and l is the length of the beam. The effective torsional stiffness of the beams is given by

$$K_T = \frac{2GJ}{l} \tag{10}$$

where G is shear modulus that can be obtained as $G = E/2(1+\nu)$ and J is the polar moment of inertia of the beam cross section expressed as [Wen, Hoa, and

Kirk (2004)]

$$J = \begin{cases} hw^3 \left[\frac{1}{3} - 0.21\frac{w}{h}\left(1 - \frac{w^4}{12h^4}\right)\right] & for\ w \le h \\ hw^3 \left[\frac{1}{3} - 0.21\frac{h}{w}\left(1 - \frac{h^4}{12w^4}\right)\right] & for\ w \ge h \end{cases} \tag{11}$$

The bending stiffness and torsional stiffness of the three mirrors calculated from the above equations are summarized in Table 3. It is shown that Mirror C has a significantly lower bending stiffness and a higher torsional stiffness compared to Mirror B. Therefore, Mirror C, has a much larger bending deformation that gets reflected in the magnitude of residual bending oscillations.

5 Computational Input Shaping Optimization

As discussed in Section 4, for mirror designs that have a low bending/torsional stiffness ratio and/or low torque/pulling force ratio, the residual oscillations due to the bending mode can be large with the step-shaped input voltage. To resolve this issue, we employ an optimization technique along with the numerical model. In order to find the correct shape of the input voltage, we seek to minimize the magnitude of the angular acceleration according to the real time dynamic response of the mirror. In this optimization problem, the objective function is simply the magnitude of the angular acceleration of the mirror plate. The angular acceleration of the mirror plate is represented by using a line connecting two nodal points p and q, one on the edge and the other at the center of the mirror plate. The nodal points are chosen such that the line connecting them is perpendicular to the longitudinal axis of the suspension beams. For the small rotation angle of the mirror plate, θ can be written as

$$\theta = \frac{w^p - w^q}{a/2} \tag{12}$$

where w^p and w^q are the vertical displacements of nodal points p and q, respectively, and a is the width of the mirror plate. The optimization problem is then

$$min\ \left|\ddot{\theta}_{n+1}(V,t)\right| = min\ \left|\ddot{w}^p_{n+1}(V,t) - \ddot{w}^q_{n+1}(V,t)\right| \qquad \text{subject to Eqs. (2-4,6)} \tag{13}$$

where the voltage V is the single input to the system to be computed for time step $n+1$ and Eqs. (2-4,6) are the coupled nonlinear system equations. Numerical methods such as the Newton methods or more recently developed fictitious time integration methods [Liu and Atluri (2008); Ku, Yeih, Liu, and Chi (2009)] are available to find an input voltage V that minimizes $|\ddot{w}^p_{n+1}(V,t) - \ddot{w}^q_{n+1}(V,t)|$. In

this work, for the sake of simplicity, we employ the standard bisection method described in [Heath (1997)].

Figures 16-18 show the optimized shape of input voltage for the three mirrors. For Mirror A, the optimized shape is nearly identical to the step-shaped input voltage. The optimization process automatically reproduces the step-shaped input voltage when the residual vibration is small. The optimization process results in a periodic input voltage design for both Mirror B and Mirror C. The period of the resulting voltage is equal to the period of the residual oscillations due to the bending mode suggesting that the computed variation of the input voltage is for compensating the bending vibration of the mirror. From a control point of view, one can think of input-shaping as zero pole cancellation method. When a single-mode is considered, a double-step voltage of the correct magnitude essentially produces a zero to cancel that pole. When two linearly-coupled modes are present as in our case, adding more steps that produce new zero to eliminate the second mode is not effective. The reason is that the new steps will affect the location of the original zero and hence will activate the first mode again. Inherently, the optimization scheme took that into account and found that the best way to eliminate this new pole is by introducing a sinusoidal signal of the same frequency of the second mode pole, thereby producing a zero which cancels this pole. As such, as shown in Figs. 17 and 18, the bending mode effect is effectively suppressed by the new optimized input voltage for both Mirrors B and C.

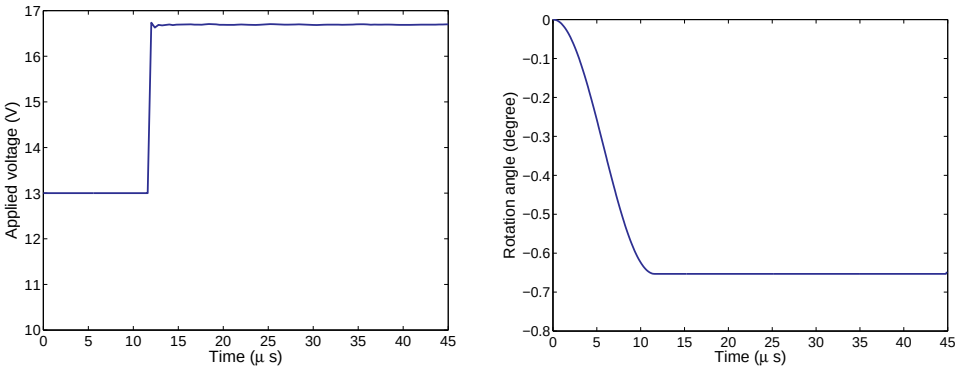

Figure 16: Input voltage optimization for Mirror A. Left: optimized input voltage. Right: dynamic response of the micromirror.

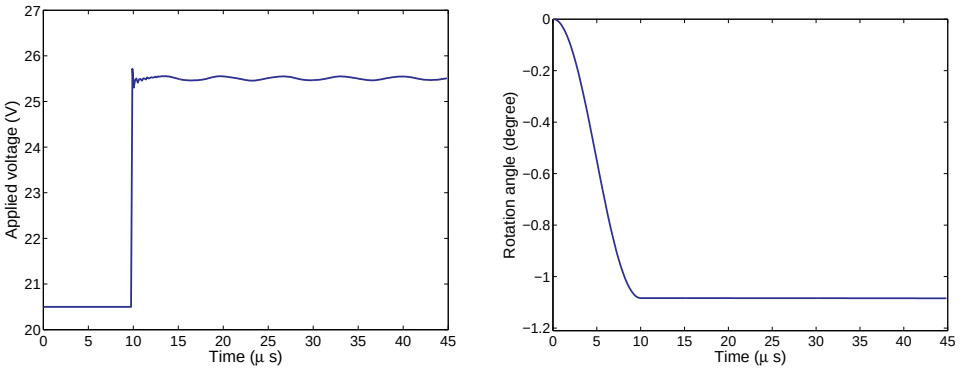

Figure 17: Input voltage optimization for Mirror B. Left: optimized input voltage. Right: dynamic response of the micromirror.

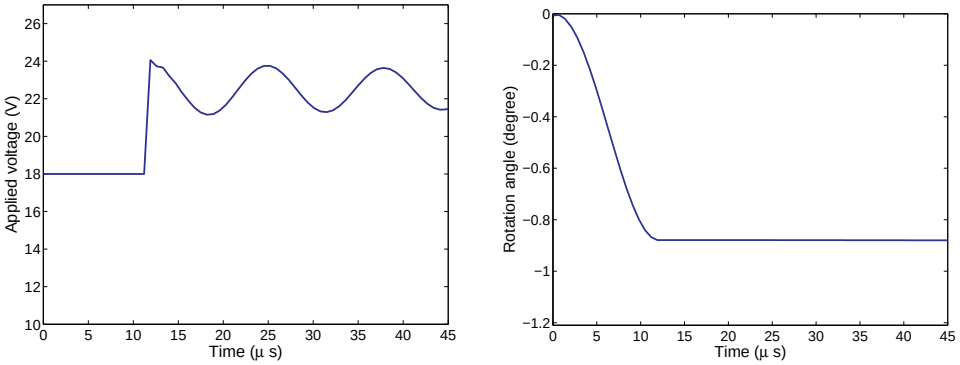

Figure 18: Input voltage optimization for Mirror C. Left: optimized input voltage. Right: dynamic response of the micromirror.

6 Conclusion

In this work, we perform computational analysis of input-shaping open-loop control of electrostatic micromirrors. We show that the higher vibrational modes may have a significant effect on the residual vibrations of the system depending on the design parameters. The significance of the bending mode effect depends on the bending/torsional stiffness ratio and the torque/bending force ratio. We employ a numerical optimization procedure to shape the input voltage from the real time dynamic response of the mirror structures. The optimization procedure results in a periodic nonlinear input voltage that can effectively suppress the bending mode effect. Our results suggest that the periodic variation of the input voltage is for

compensating the bending vibration of the mirror.

Acknowledgement: We gratefully acknowledge support by the Clemson University start-up funds.

References

Aliabadi, M. H.; S.Hall, W. (1985): Taylor expansions for singular kernels in the boundary element method. *International Journal for Numerical Methods in Engineering*, vol. 21, pp. 2221–2236.

Aliabadi, M. H.; S.Hall, W. (1989): The regularising transformation integration method for boundary element kernels. comparison with series expansion and weighted gaussian integration methods. *Engineering Analysis with Boundary Elements*, vol. 6, pp. 66–71.

Bettini, P.; Brusa, E.; Munteanu, M.; Specogna, R.; Trevisan, F. (2008): Innovative numerical methods for nonlinear MEMS: the non-incremental FEM vs. the discrete geometric approach. *CMES: Computer Modeling in Engineering & Sciences*, vol. 33, no. 3, pp. 215–242.

Borovic, B.; Hong, C.; Liu, A.; Xie, L.; Lewis, F. (2005): Control of a MEMS optical switch. In *43rd IEEE Conference on Decision and Control*.

Borovic, B.; Liu, A.; Popa, D.; Cai, H.; Lewis, F. (2005): Open-loop versus closed-loop control of MEMS devices: choices and issues. *Journal of Micromechanics and Microengineering*, vol. 15, no. 1-2, pp. 1917–1924.

Chen, C. K.; Lai, H. Y.; Liu, C. C. (2009): Nonlinear micro circular plate analysis using hybrid differential transformation/finite difference method. *CMES: Computer Modeling in Engineering & Sciences*, vol. 40, no. 2, pp. 155–174.

Cook, R. D.; Malkus, D. S.; Plesha, M. E.; Witt, R. J. (2001): *Concepts and Applications of Finite Element Analysis*. J. Wiley & Sons.

Daqaq, M. F.; Reddy, K. C.; Nayfeh, A. H. (2008): Input-shaping control of nonlinear MEMS. *Nonlinear Dynamics*, vol. 54, no. 1-2, pp. 167–179.

He, X.; Lim, K. M.; Lim, S. P. (2008): Fast BEM solvers for 3D poisson-type equations. *CMES: Computer Modeling in Engineering & Sciences*, vol. 35, no. 1, pp. 21–48.

Heath, M. T. (1997): *Scientific computing: an introductory survey*. McGraw-Hill.

Hyde, J. M. (1991): Multimode vibration suppression in controlled flexible systems. Master's thesis, MIT, Cambridge, MA, 1991.

Judy, J. (2001): Microelectromechanical systems (MEMS): Fabrication, design, and applications. *Smart Materials and Structures*, vol. 10, pp. 1115–1134.

Ku, C. Y.; Yeih, W.; Liu, C. S.; Chi, C. C. (2009): Applications of the fictitious time integration method using a new time-like function. *CMES: Computer Modeling in Engineering & Sciences*, vol. 43, no. 2, pp. 173–190.

Li, G.; Aluru, N. R. (2001): Linear, nonlinear and mixed-regime analysis of electrostatic MEMS. *Sensors and Actuators*, vol. 91, pp. 278–291.

Li, G.; Aluru, N. R. (2002): A lagrangian approach to compute electrostatic forces on deformable mems. *Journal of Microelectromechanical Systems*, vol. 11, no. 3, pp. 245–254.

Li, G.; Aluru, N. R. (2003): Efficient mixed-domain analysis of electrostatic MEMS. *IEEE Transactions on Computer-Aided Design of Integrated Circuits and Systems*, vol. 22, no. 9, pp. 1228–1242.

Lin, S. M. (2009): Vibration suppression of a moving beam subjected to an active-control electrostatic force. *CMES: Computer Modeling in Engineering & Sciences*, vol. 43, no. 1, pp. 73–90.

Liu, C. S.; Atluri, S. N. (2008): A novel time integrationmethod for solving a large system of non-linear algebraic equations. *CMES: Computer Modeling in Engineering & Sciences*, vol. 31, no. 2, pp. 71–83.

Mukherjee, T. (2000): Emerging simulation approaches for micromachined devices. *IEEE Trans. Computer-Aided Design*, vol. 19, pp. 1572–1589.

Popa, D. O.; Byoung, H. K.; Wen, J. T.; Stephanou, H. E.; Skidmore, G.; Geisberger, A. (2003): Dynamic modeling and input shaping of thermal bimorph MEMS actuators. *Proceedings of IEEE International Conference on Robotics and Automation*, vol. 1, pp. 1470–1475.

Rewienski, M.; White, J. (2003): A trajectory piecewise-linear approach to model order reduction and fast simulation of nonlinear circuits and micromachined devices. *IEEE Transactions on Computer-Aided Design of Integrated Circuits and Systems*, vol. 22, no. 2, pp. 155–170.

Shi, F.; Ramesh, P.; Mukherjee, S. (1995): On the application of 2D potential theory to electrostatic simulation. *Communications in Numerical Methods in Engineering*, vol. 11, pp. 691–701.

Singer, N. C.; Seering, W. P. (1990): Preshaping command inputs to reduce system vibration. *Journal of Dynamic Systems, Measurement, and Control*, vol. 112, pp. 76–82.

Wen, J.; Hoa, X. D.; Kirk, A. G. (2004): Analysis of the performance of a MEMS micromirror. *IEEE Transations on Magnetics*, vol. 40, no. 2, pp. 1410–1413.

Yang, T.; Chen, K.; Lee, C.; Yin, J. (2006): Suppression of motion-induced residual vibration of a cantilever beam by input shaping. *Journal of Engineering Mathematics*, vol. 54, no. 1, pp. 1–15.